# In situ control of oxygen partial pressure in a buffered UO2 fuel: A manufacturing process

Mira Khair, Chantal Riglet-Martial, Pierre Matheron, Jacques Léchelle, Hervé Palancher, Xavière Iltis, Nicolas Tarisien, Jean-Marc Heintz

# *In situ* control of oxygen partial pressure in a buffered $UO_2$ fuel: A manufacturing process

M. Khair[1 2]*, Ch. Riglet-Martial[1], P. Matheron[1], J. Lechelle[1], H. Palancher[1], X. Iltis[1], N. Tarisien[1], J-M Heintz[2].

[1] CEA, DEN, DEC, Centre d'Etudes de Cadarache - 13108 Saint-Paul-lez-Durance Cedex - France

[2] Univ. Bordeaux, CNRS, Bordeaux INP, ICMCB, UMR 5026, F-33600 Pessac, France

***Keywords**:* Molybdenum, Niobium, Uranium, Oxide, Fuel, dopant, Thermodynamics, Oxido-reduction, Oxygen buffer, Redox buffer, $O_2$ regulation.

* Corresponding author's e-mail: mira.khair@u-bordeaux.fr

**Abstract**

An innovative laboratory process making use of the specific properties of solid redox buffers was developed for producing $O_2$ self-regulated $UO_2$ fuel samples. The method was optimized using Molybdenum and Niobium oxide buffers. The starting materials were first mixed with the $UO_2$ powder, then pressed into pellets and finally sintered in a quasi-closed vessel at 1670°C under strictly controlled oxygen potential using appropriate solid redox buffers. Speciation of Mo and Nb was characterized using Scanning Electron Microscopy (SEM) combined with Energy Dispersive X-ray spectroscopy (EDX) as well as X-ray Diffraction (XRD). Using this optimized procedure, both oxido-reducing forms of the $O_2$ buffer incorporated into the $UO_2$ specimens were preserved during sintering, allowing an *in situ* control of the $O_2$ partial pressure inside the material. The processing methodology, the laboratory experimental set-up, the sintering procedure and the characteristics of the final oxygen buffered $UO_2$ fuel are described. This work opens the path to representative laboratory studies related to the redox dependent behavior of irradiated fuels in reactor.

# 1. Introduction

In nuclear reactors fed with oxide fuels, important properties of the fuel - such as thermal conductivity, solid-state diffusion, creep rate, volatile fission products and fission gases (such as Cs, I, Te, Xe and Kr) speciation and release - are essentially determined by temperature and oxygen partial pressure (i.e. the oxygen potential). However, this latter parameter being not strictly controlled is likely to vary noticeably both in space and time during fuel irradiation and, thus, significant changes in the macroscopic material properties as well as in the speciation of the corrosive volatile fission products, responsible for cladding fuel chemical interaction and potential cladding damage, are expected [1]–[3]. In order to reduce the possible drawbacks resulting from uncontrolled variations of oxygen potential under operation, the addition to the fuel of a solid oxido-reducing buffer as a dopant could be beneficial, as it would provide to the material a larger oxygen buffering capacity. As a result, it is assumed that oxygen buffered fuels would greatly help to better control (i.e. with a lower variability) all key properties of the material dependent on oxygen concentration (creep rate, thermal conductivity, fission gas speciation…).

The evolution of oxide fuel properties under changing oxygen potentials during irradiation is still not fully understood. In addition, research on the buffering capabilities of $O_2$ self-regulated fuel materials is even scarcer. However, an interesting application is given in reference [4] which refers to the way to reduce and control the continuous increase of free oxygen with increasing burn-up. Addition of metallic Mo to the fuel, as a dopant, is recommended in order to generate *in situ* control of the oxygen partial pressure during operation, the ($MoO_2$/Mo) redox buffer acting as an oxidizing barrier and keeping constant the oxygen potential throughout the in-reactor irradiation.

Manufacturing oxygen buffered $UO_2$ fuel samples in laboratory is far from being straightforward as both the fuel material itself and the incorporated buffers are very sensitive to oxido-reduction [5]. A very strict control of the oxygen partial pressure during sintering is absolutely required in order to preserve both oxido-reducing forms of the buffer inside the final $UO_2$ specimens. To fulfill this requirement, an innovative way in the field of nuclear fuel manufacturing consists in buffering the sintering atmosphere

with appropriate solid redox buffers, instead of the usual ($H_2O/H_2$) or ($CO_2/CO$) gaseous buffers implemented industrially. Such gaseous buffers would need a very precise control of their ratio over the entire range of temperature (20-1700°C) in a way that is quite difficult to obtain in an industrial furnace.

The aim of this work is to develop a laboratory process, making use of the specific properties of solid redox buffers to produce $O_2$ self-regulated fuel samples. The method was optimized using two types of buffers. A Molybdenum buffer was chosen first due to its presumed relevance for controlling the oxygen potential of nuclear fuel under operation [6]. A Niobium buffer was also tested for comparison, due to its various stable redox states within the expected range of variation for irradiated nuclear fuels and its possible chemical interactions with the $UO_2$ matrix. The processing methodology, the laboratory experimental set-up, the sintering procedure and the characterization of the final oxygen buffered $UO_2$ fuels are described in the present paper.

# 2. Experimental section - materials and methods

## 2.1. Concentration of additives

A preliminary estimation of the concentration of solid buffers to be added to $UO_2$ was carried out considering both the target buffering capacity of the final specimen and the $UO_2$ initial hyperstoichiometry to be balanced with the buffer. The target buffering capacity to achieve is based on previous preliminary calculations [7] (out of scope of the present study) which concluded that a buffering capacity of about 13 millimole O/mol U, both in oxidation and reduction regimes, would be necessary to balance redox perturbations applied to fuels of 50 $GWd.t^{-1}$ U burn-up, during a power transient. This leads to concentrations of about 0.54 wt% of Mo buffer powder (with equimolar solid compound (sc) amounts of $Mo_{(sc)}$ and $MoO_{2(sc)}$) and 2.48 wt% of Nb buffer powder (with equimolar amounts of $NbO_{2(sc)}$ and $Nb_2O_{5(sc)}$). All these calculations being based on the initial weight of $UO_{2,03}$.

The estimation of the additional quantity of reductant needed to balance the $UO_2$ powder initial hyperstoichiometry is based on the following redox reactions giving the conversion of $UO_{2.03}$ to $UO_{2.001}$

(which are the expected approximate stoichiometry of the buffered $UO_2$ specimen at equilibrium at 1670°C (sintering temperature) with the ($MoO_2$/Mo) and ($Nb_2O_5$/$NbO_2$) buffers respectively), assuming that the buffers do not interact with the $UO_2$ matrix:

$$UO_{2.03} + \frac{0.029}{2} Mo \rightarrow UO_{2.001} + \frac{0.029}{2} MoO_2 \quad (1)$$

$$UO_{2.03} + 0.058\, NbO_2 \rightarrow UO_{2.001} + 0.029\, Nb_2O_5 \quad (2)$$

Equations (1) and (2) indicate that additional concentrations of about 0.51 wt% $Mo_{(sc)}$ and 2.7 wt% $NbO_{2(sc)}$ would be required to balance the initial $UO_2$ hyperstoichiometry (all values related to the initial weight of $UO_{2.03}$).

Overall, from this preliminary analysis, the approximate concentrations of solid buffers would be of about 1.04 wt% of a $MoO_2$/Mo mixture (including 0.30 wt% $MoO_2$ and 0.74 wt% Mo) and 5.17 wt% of a $Nb_2O_5$/$NbO_2$ mixture (including 1.28 wt% $Nb_2O_5$ and 3.89 wt% of $NbO_2$).

However, it is obvious from back-experience that large amounts of additives of Niobium (> 2 wt%) are likely to cause an undesirable deterioration (cracking) of the $UO_2$ pellets [5] during its fabrication. Thus, the previous analysis clearly implies that the manufacturing of $UO_2$ pellets doped with the ($Nb_2O_5$/$NbO_2$) buffer cannot be carried out on a single step, for the initial $UO_{2.03}$ powder, without the help of an extra independent reducing agent. A pre-reduction stage (for example) of the $UO_{2.03}$ powder would be necessary before incorporating the Niobium buffer. In addition, a total amount of 2.48 wt% Nb buffer powder (with equimolar Nb amounts of $NbO_{2(sc)}$ and $Nb_2O_{5(sc)}$) to achieve the target buffering capacity is not necessary from an experimental point of view to demonstrate the validity of the process and the capability of this fuel buffering.

In this framework, different dopant amounts were tested in order to determine the experimental conditions leading to the best compromise between low degradation of the sintered pellets, significant buffer capacity

and reduction of $UO_{2.03}$. The experimental conditions selected in the present study are gathered in **Table 1**. The Mo or Nb buffers powders were mixed with the initial $UO_{2.03}$ powder in total concentrations of 2 wt% for Molybdenum and 0.8 and 1.6 wt% for Niobium. Pellets doped with the ($MoO_2$/Mo) buffer were sintered under a flow of Argon. Those doped with the ($Nb_2O_5$/$NbO_2$) buffer were sintered under three different gas streams: Ar, Ar/2% $H_2$ and Ar/5% $H_2$.

| **Sample** | 1 | 2 | 3a | 3b | 3c | 4a | 4b | 4c |
|---|---|---|---|---|---|---|---|---|
| **Additive** | $MoO_2$/Mo | Mo | $Nb_2O_5$/$NbO_2$ | | | | | |
| **wt%** | 2 (0.5/1.5) | 2 | 0.8 (0.4/0.4) | | | 1.6 (0.8/0.8) | | |
| **Atmosphere** | Ar | Ar | Ar | Ar 2%$H_2$ | Ar 5%$H_2$ | Ar | Ar 2%$H_2$ | Ar 5%$H_2$ |
| **Aim** | To test the effect on density | To validate the hypothesis of the $UO_2$ reduction by Mo | Same concentration conditions as literature [5] | | | To test the effect of concentration on density | | |

## 2.2. Sample preparation

The procedure of preparation of $UO_2$ pellets with redox buffer is similar to conventional powder metallurgy processes: mixing, pelletizing, and sintering.

The starting uranium oxide was a $UO_{2.03}$ powder whose stoichiometry was precisely controlled by thermogravimetry (TGA). The powders used for the buffers were Mo metallic powder (Aldrich 99.9%,) and $MoO_2$ powder (Alfa Aesar 99%) for Molybdenum, and $NbO_2$ (Aldrich 99.99%) plus $Nb_2O_5$ (Prolabo 99.99%) for Niobium. The mixed powders were then placed in a planetary mixer (FRITSCH Pulverisette Analysette Laborette) in order to obtain an intimate and homogeneous mixture. The speed of

rotation of the mixer was set to 250 rpm and the duration of powder mixing was limited to 15 minutes to avoid further oxidization of $UO_2$ due to the temperature increase relative to grinding.

In a second step, the mixed powders were compacted with a double-effect uniaxial press at 450 MPa. The green densities of the pellets (densities before sintering), expressed in % of the theoretical density (thd) were as follows:

- 6.08 ±0.06 (55.5 thd%) for the samples with 2 wt% Mo
- 6.06 ±0.08 (55.3 thd%) for the samples with 0.5 wt% $MoO_2$/1.5 wt% Mo
- 6.08 ±0.08 (59.2 thd%) for the samples with 0.8 wt% $Nb_2O_5/NbO_2$
- 6.01 ±0.01 (58.9 thd%) for the samples with 1.6 wt% $Nb_2O_5/NbO_2$

In the final step, detailed in the next paragraph, the samples were sintered with an objective of reaching a densification close to 95 thd%.

## 2.3. Sintering process

The sintering of the doped $UO_2$ pellets had to be carried out in an atmosphere with controlled $O_2$ partial pressure in order to preserve the two oxido-reducing forms of the oxygen buffer inside the samples. This was achieved by controlling the $O_2$ partial pressure during sintering with "external" solid oxygen buffers, using an experimental set-up derived from that described in references [8]–[10].

The operating principle of the system is as follows: the $MO_x/MO_y$ external buffer is exposed to a continuous flow of inert gas of high purity (Ar 99.998 % or better). Depending on its temperature, the buffer may release or absorb oxygen from the gas stream due to the change in the equilibrium of the redox reaction between materials of different degrees of oxidation. This mechanism works as long as there are sufficient quantities of both components of the external buffer. Therefore, the oxygen partial pressure in the atmosphere should be close to this equilibrium (quasi steady state).

So, the sintering was carried out by heating the doped $UO_2$ samples together with the same buffer system as that enclosed in the specimen, in a tungsten semi-closed vessel. **Fig. 1** shows the schematic drawing of

the experimental set-up. The buffered $UO_2$ pellets were placed in the upper part of the vessel. To control the $pO_2$ during experiments, equimolar powders mixtures of $Nb_2O_5/NbO_2$ or $MoO_2/Mo$ were employed as oxygen buffers and were placed in the lower part. Both parts communicate with an aperture allowing the buffer powder mixture to control the $O_2$ partial pressure in the whole vessel. The three parts of the device, including the cover, were not welded together, hence the name "semi-closed system". The whole experimental set-up was integrated into an alumina tubular furnace and the following sintering cycle was applied under a continuous gas stream (100 L/h): heating at 130°C.h$^{-1}$, plateau at 1670°C during 3 hours and cooling at 150°C.h$^{-1}$. Moreover, a powder sample of the same buffer system as that enclosed in the vessel was also placed at the entrance of the furnace in order to verify the impact of the gas stream on the buffer **(Fig .1).** After sintering, as long as both phases remain present in the internal and external buffer, we assume that the oxygen buffer was large enough to control the oxygen potential at the equilibrium of the respective reaction in the crucible and/or furnace. The four different types of samples (1 to 4) were sintered independently under different atmospheres. The $UO_2$ pellets doped with the ($MoO_2/Mo$) buffer were sintered under a flow of Argon. The sintering of the pellets doped with the ($Nb_2O_5/NbO_2$) buffer was carried out in three different experiments under three different gas streams: Ar, Ar/2% $H_2$ and Ar/5% $H_2$.

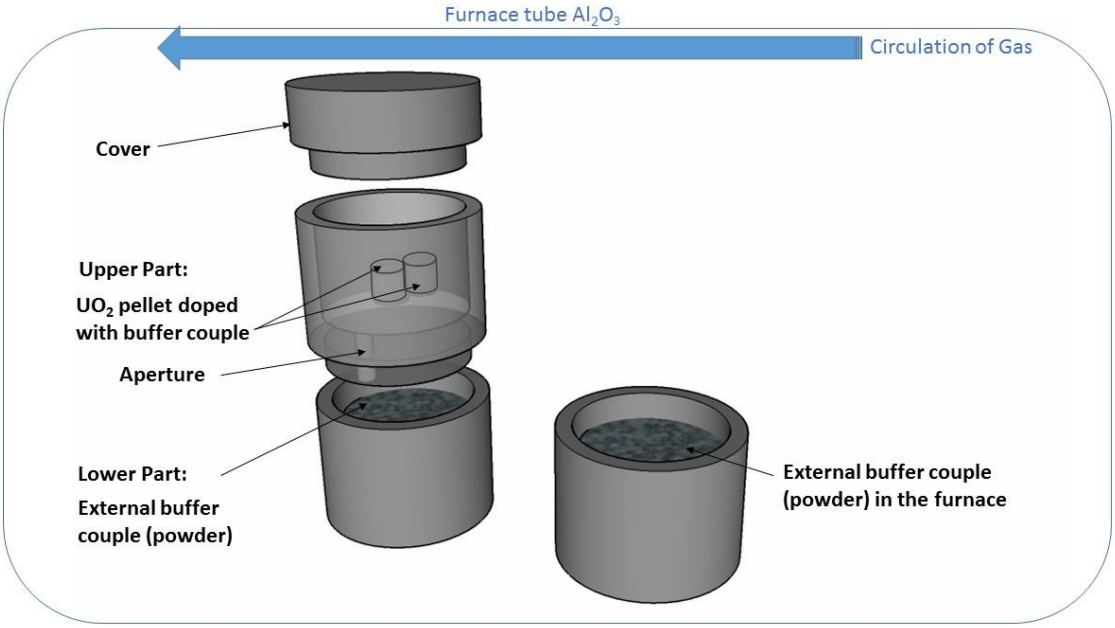


**Figure 1:** Schematic representation of the experimental set-up (Tungsten crucible + furnace) used for sintering

## 2.4. Characterization methods

The density of the green and sintered pellets were measured geometrically and reported as a percentage of the theoretical density considering the amounts of Niobium and Molybdenum added to the pellets. After sintering, the samples were sliced longitudinally and mechanically polished, with a diamond suspension finish (1 µm grade). The slices were then analyzed using Scanning Electron Microscopy (SEM) (FEI Nova NanoSEM 450) combined with Energy Dispersive X-ray spectroscopy (EDX) and Electron Backscatter Diffraction (EBSD) (both from Oxford Instruments) in order to study the Molybdenum and Niobium distribution in the pellets as well as the chemical composition and the grain size. In addition, an X-ray diffraction analysis was performed on the used external powder buffers both in the crucible and in the furnace. XRD spectra were measured for 2θ ranging from 20° to 90° with a Bruker D8 Advance diffractometer (with anti- cathode Cu-Kα) and the lattice parameters of oxides were calculated using the TOPAS software. All counting intensities were transformed to square root in order to reduce the intensity of the majority phase peaks compared to the minority, and hence aid with comparison.

# 3. Experimental results

## 3.1. Density of the pellets

**Table 2** summarizes the densities of $UO_2$ pellets doped with ($MoO_2$/Mo) and ($Nb_2O_5$/$NbO_2$) buffers. Whatever the dopant added, the sintered densities remain lower than the target density of 95 thd%. Under Argon, the buffer impact on density is higher with Nb than with Mo, in spite of a lower added amount. The Mo doped pellets (Samples 1 and 2) have a density close to 90.7 thd%, against only about 88.5 thd% for Nb doped ones (Samples 3 and 4).

Considering the effect of the sintering atmosphere for the pellets doped with the two amounts of $Nb_2O_5$/$NbO_2$ buffer (Samples 3 and 4), a contrasting behavior can be noted. An increase in the final density is observed for sample 3 (lowest doping amount: 0.8 wt%) when pO2 is decreasing while the density remains almost constant and low for sample 4 (1.6 wt%). Sample 3 contradicts previously published studies where either $NbO_2$ or $Nb_2O_5$ was added to $UO_2$ separately, with different amounts (0.5 wt % max) and sintered in different atmospheres: $H_2$/$H_2O$ or CO/$CO_2$ [11]–[14]. These studies showed that the density of $UO_2$ pellets increased with $pO_2$ in the atmosphere. Our results appear rather in agreement with another study [5] which showed a decrease in density (88 % dth) with an increase of pO2, which was interpreted as the consequence of a de-densification phenomenon.

In fact, for Samples 3 and 4, the gaseous surrounding environment of the pellets must be taken into account as it is partially imposed by the external buffer of the lower part of the crucible. But, since our system is semi-closed, the gas stream in the furnace can also slightly modify the $pO_2$ around the pellets. This could explain the lack of connection between the $pO_2$ of the gas stream and the final density of the doped pellets.

The density of the sintered pellets is in all cases (**Table 2**) lower than the initial target value (95 thd%). Although the density could be improved by using lower quantities of additives, the obtained densities were considered as satisfactory for the sake of our study.

| Sample | wt% of dopants | Theoretical Density | Geometrical relative density (thd%) | | |
|---|---|---|---|---|---|
| | | | Ar | Ar/2%$H_2$ | Ar/5%$H_2$ |
| **1** | 0.5 wt% $MoO_2$ / 1.5 wt% Mo | 10.95 | 90.8 | - | - |
| **2** | 2.0 wt% Mo | 10.94 | 90.6 | - | - |
| **3** | 0.4 wt% $Nb_2O_5$ / 0.4 wt% $NbO_2$ | 10.92 | 88.6 | 90.3 | 83.8 |
| **4** | 0.8 wt% $Nb_2O_5$ / 0.8 wt% $NbO_2$ | 10.86 | 88.2 | 86.0 | 87.5 |

## 3.2. Characterization of the samples

### 3.2.1. $UO_2$ pellets buffered with ($MoO_2$/Mo)

**Fig. 2** presents the X-ray diffraction patterns obtained on the $MoO_2$/Mo powder mixtures, respectively placed in the tungsten crucible and in the furnace. Rietveld analyses of these patterns indicate that the process ended up with 23.5 wt% Mo and 76.5 wt% $MoO_2$ in the tungsten crucible [diffractogram in black] and with 32.6 wt% Mo and 67.4 wt% $MoO_2$ in the furnace [diffractogram in red], as compared to the initial (equimolar) composition of 42.9 wt% Mo and 57.1 wt% $MoO_2$. The results show that Mo metal of the buffer inside the furnace partially oxidized during sintering, which suggests that the buffer contributed to purify the Argon flow entering the vessel, by decreasing the $O_2$ partial pressure toward that imposed by the ($MoO_2$/Mo) redox couple. The buffer inside the W crucible also partly oxidized during sintering, which suggests that part of it contributed to reduce the initial uranium $UO_{2.03}$ matrix of the pellets.

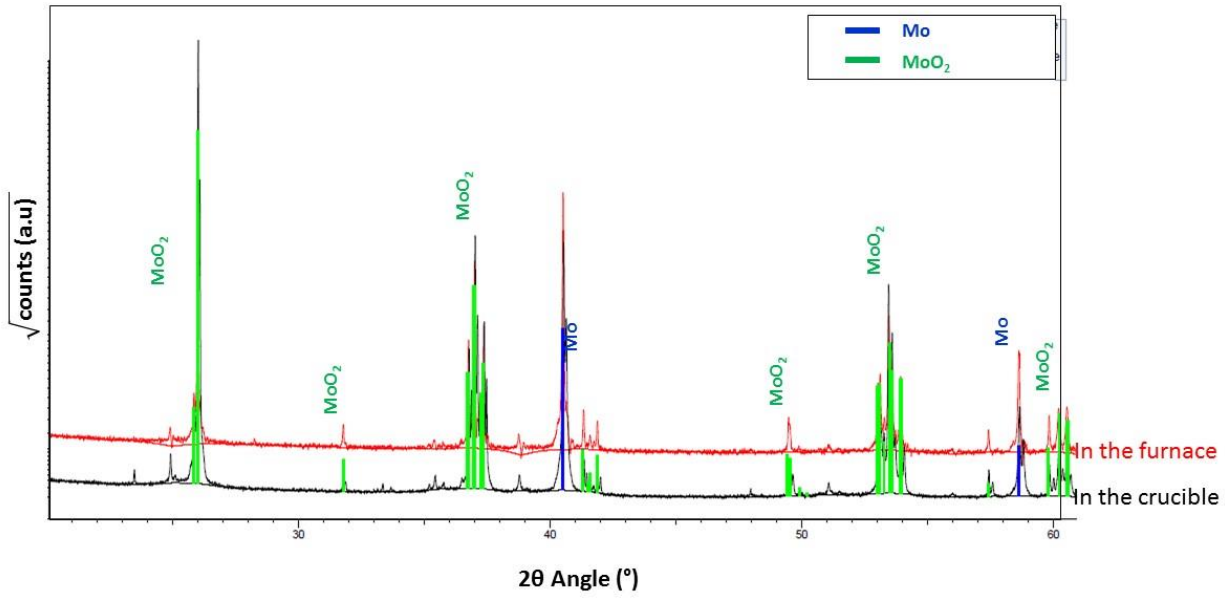


**Figure 2 :** X-ray diffraction patterns of $MoO_2$/Mo powders sintered 3 h at 1670°C under Ar in the furnace (red curve) and in the tungsten crucible (black curve). In the Y axes, the square root of the diffracted intensities is given.

**Fig. 3** (parts a & b) shows the SEM micrographs of the $UO_2$ pellet doped with 0.5 wt% $MoO_2$/1.5 wt% Mo (Sample 1) and 2 wt% Mo (Sample 2) respectively. The SEM images clearly show homogenous overall microstructures, in terms of porosity and precipitates density, free from cracks, with three different shades of grey corresponding to three different compositions. The light grey shade corresponds to $UO_2$, while the medium and dark grey shades refer to precipitates containing Molybdenum with two different oxidation forms. The different kinds of phases could be distinguished by different gray levels from the Backscattered Electron Image (BEI).

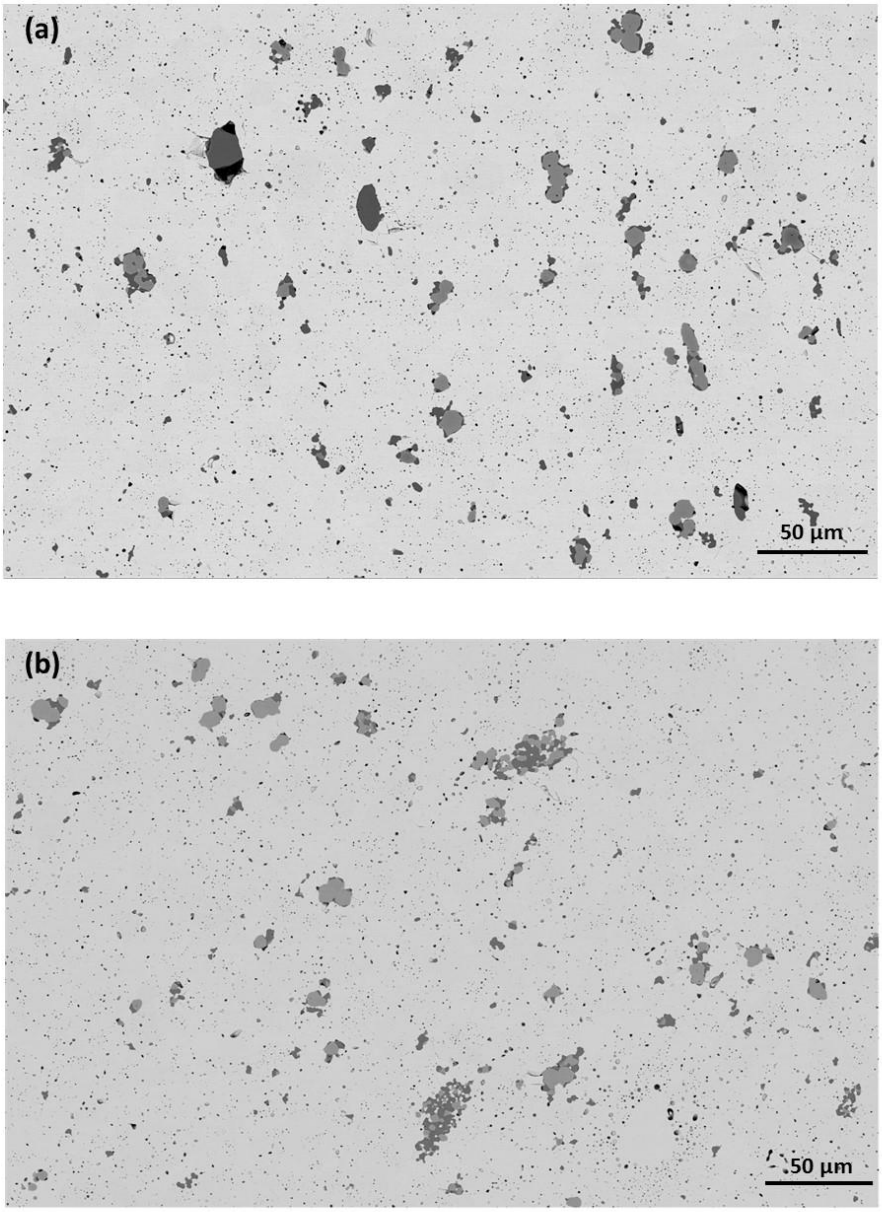


**Figure 3:** SEM images of (a) Sample 1 ($UO_2$ pellet doped with **0.5 wt% $MoO_2$/1.5 wt% Mo**) and (b) Sample 2 ($UO_2$ pellet doped with **2 wt% Mo**), both sintered 3 h at 1670°C in Ar.

Indeed, as an example, the EDX analyses performed on Sample 2 (doped with 2 wt% Mo), along a line scan crossing the three phases (**Fig. 4**) show that Mo contents corresponding to almost 100 at% Mo (neglecting a low oxygen amount, of a few at%, probably due to a superficial oxidation) and 35-37 at% Mo, are measured in the medium grey areas and in the dark grey area respectively. These results indicate that these two Mo-rich phases probably correspond to almost pure Mo (medium grey areas) and $MoO_2$ (dark grey areas). Punctual analyses were performed on different precipitates (100 points per sample) and confirmed these observations.

Then, SEM -EDX maps of both Samples 1 and 2 were processed using the ImageJ software in order to determine $MoO_2$/Mo weight fractions.

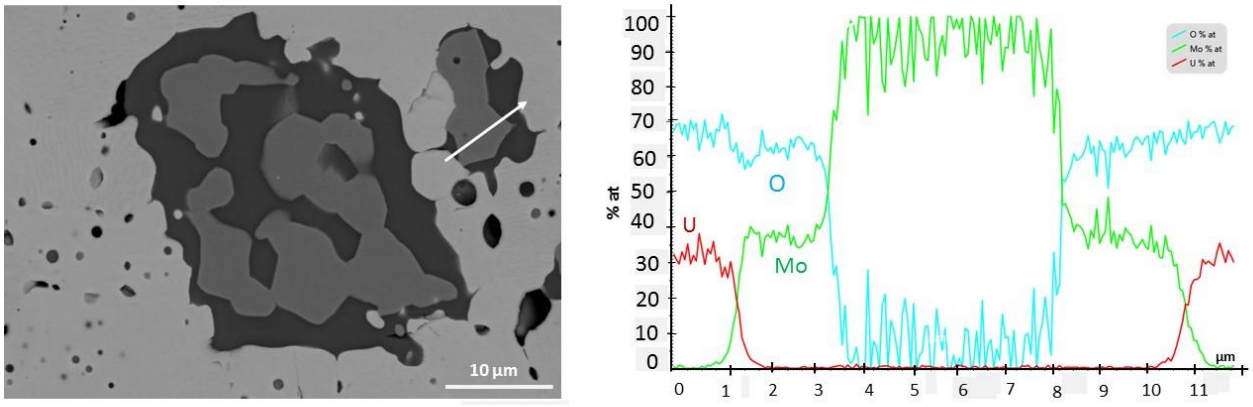


**Figure 4** : EDX line scan analysis of Sample 2 ($UO_2$ pellet doped with **2 wt% Mo**) sintered 3 h at 1670°C in Ar.

The elemental compositions of each $UO_2$ doped molybdenum pellet and buffer couple are given in Table 3.

| Sample | Atmosphere | Buffer powder in the furnace (XRD) | Buffer powder in the crucible (XRD) | Precipitates in the pellet (EDX) |
|---|---|---|---|---|
| 1 and 2 | Ar | 23.5 % wt $MoO_2$/ 76.5 % wt Mo | 32.6 % wt $MoO_2$/ 67.4 % wt Mo | $MoO_2$/Mo |

By adjusting the gray level threshold in the area of interest, $UO_2$ matrix, porosity, dark gray precipitates ($MoO_2$) and light gray precipitates (Mo) could be clearly distinguished. The total area of each gray level was then quantified and processed (determination of the ratio of areas of Mo and $MoO_2$ phases), as it is shown in **Fig. 5**. Since a great number of precipitates has been analyzed and considering that the precipitates are isotropic, the ratio of the surface fraction of each of these two phases should be identical to the volume ratio of these two phases. The volume ratio was then corrected from density of Mo and $MoO_2$ to get a weight ratio.

The co-existence of both redox forms of Mo in the crucible and inside the pellets, confirms that the $O_2$ partial pressure was stabilized to that of the ($MoO_2$/Mo) redox buffer at the end of the process, which suggests that thermodynamic equilibrium was reached.

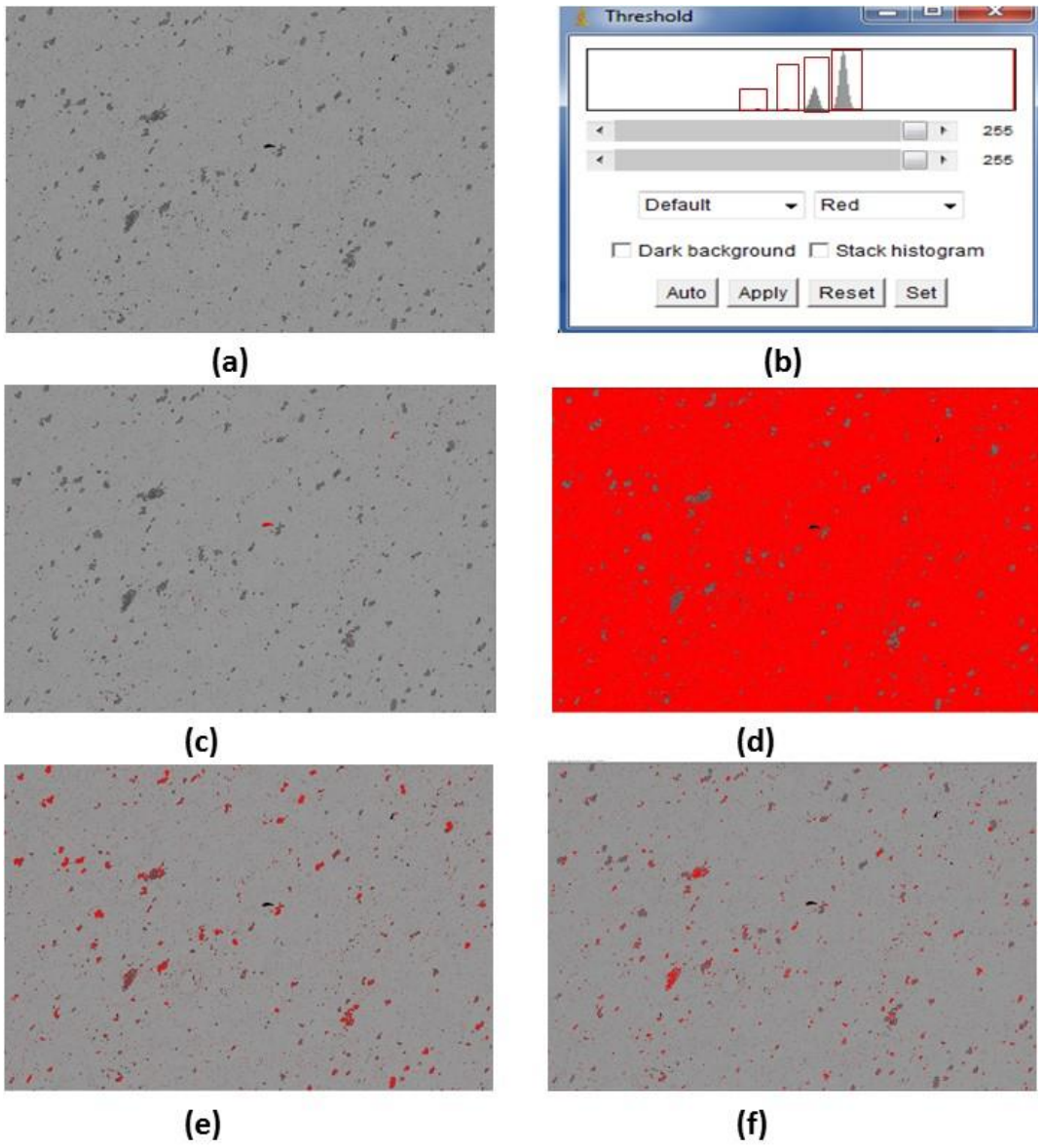


**Figure 5**: Different steps of the micrograph image analysis for determination of the surface fraction of each component in Sample 2 ($UO_2$ pellet doped with **2% Mo**): (a) SEM image, (b) definition of the thresholds (c) porosity, (d) $UO_2$ matrix, (e) $MoO_2$ precipitates (in dark grey in (a)) and (f) Mo precipitates (in medium grey in (a)).

The results show, for the two samples after sintering, the same ratio between the quantities of $MoO_2$ and Mo precipitates ($MoO_2$/Mo = 0.5 ± 0.1 wt%). Hence, it confirms the reduction of $UO_{2.03}$ by Mo throughout

the process. Moreover, the coexistence of Mo and $MoO_2$ precipitates inside the pellets after sintering suggests that the $O_2$ partial pressure has been maintained *in situ* by the ($MoO_2$/Mo) redox buffer throughout the fabrication process.

Furthermore, by analyzing by EBSD the light grey phase in **Fig. 3**, the $UO_2$ grain size, defined as the equivalent circle diameter, was found to be roughly 14 µm, which is close to the conventional grain size of $UO_2$ sintered in the same conditions (~ 10 µm).

### 3.2.2. $UO_2$ pellets buffered with ($Nb_2O_5$/$NbO_2$)

#### 3.2.2.1. Sintering under Ar atmosphere

**Fig. 6** shows the X-ray diffraction patterns of the Niobium powder buffers present in the crucible [diffractogram in blue] and inside the furnace [diffractogram in black], at the end of the sintering process under Ar atmosphere. The blue diffractogram in **Fig. 6** shows the presence in the crucible of both $NbO_2$ and sub-stoichiometric $Nb_2O_{5-x}$ compounds ($Nb_{12}O_{29}$ and $NbO_{2.432}$) after sintering. The $Nb_{12}O_{29}$ and $NbO_{2.432}$ formula (instead of the initial $Nb_2O_5$) refers to nonstoichiometric compounds close to $Nb_2O_{5-x}$ ($0 < x < 0.1$) including many stable and metastable phases [15]–[17]. The coexistence of two oxides (mainly $NbO_2$ and $NbO_{2.432}$) with two different oxidation states confirms that the $O_2$ partial pressure of the gas inside the crucible was stabilized in the vicinity of the ($NbO_{2.432}$/$NbO_2$) redox buffer during the process. Moreover, as shown in the black diffractogram in **Fig. 6**, the same phases were present in the buffer placed in the furnace.

So, powder buffers introduced in the furnace or inside the crucible both exhibit the two $NbO_2$ and $Nb_2O_{5-x}$ compounds, which implies that the $O_2$ partial pressure was kept stable. This also suggests that the final equilibrium state (between pellets and atmosphere) was reached.

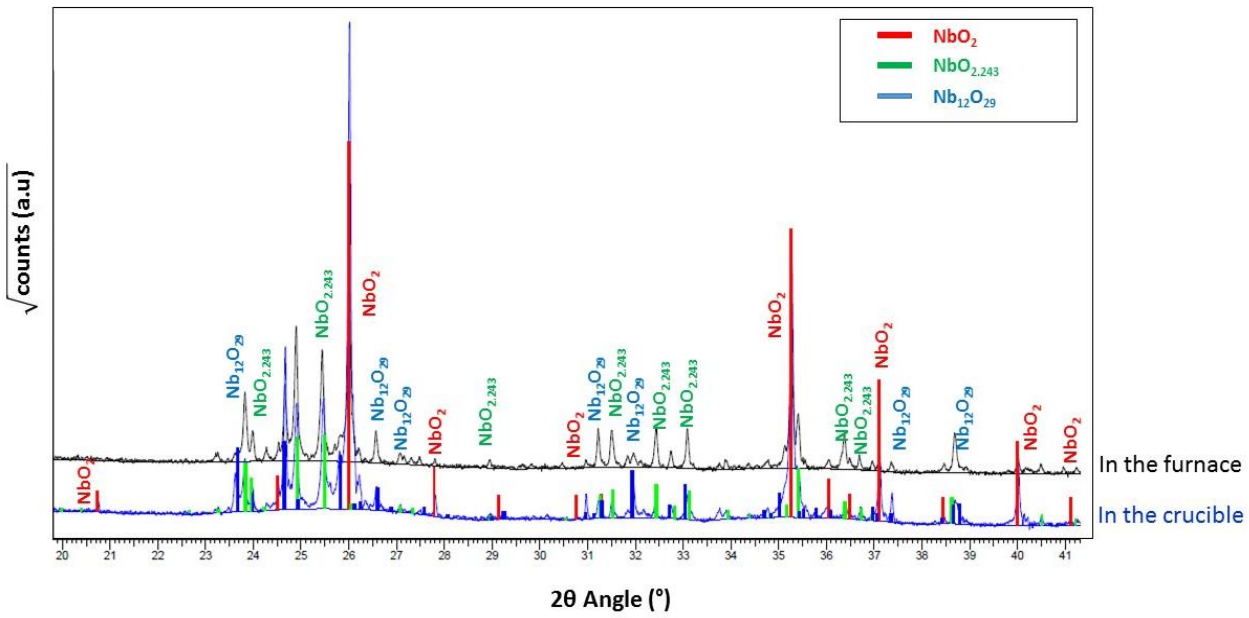


**Figure 6**: X-ray diffraction patterns for **$Nb_2O_5$/$NbO_2$ powders** sintered 3 h at 1670°C under Ar in the furnace (black curve) and in the tungsten crucible (blue curve)**.** In the Y axes, the square root of the diffracted intensities is given.

**Fig. 7 (part a & b)** shows two SEM micrographs of samples 3a and 4a ($UO_2$ pellets doped with 0.8 and 1.6 wt% Nb respectively) and sintered at 1670°C in an Ar atmosphere. The SEM images (**Fig. 7**) clearly show a single shade of grey throughout the precipitates, which tends to indicate the presence of a single homogeneous Niobium oxide.

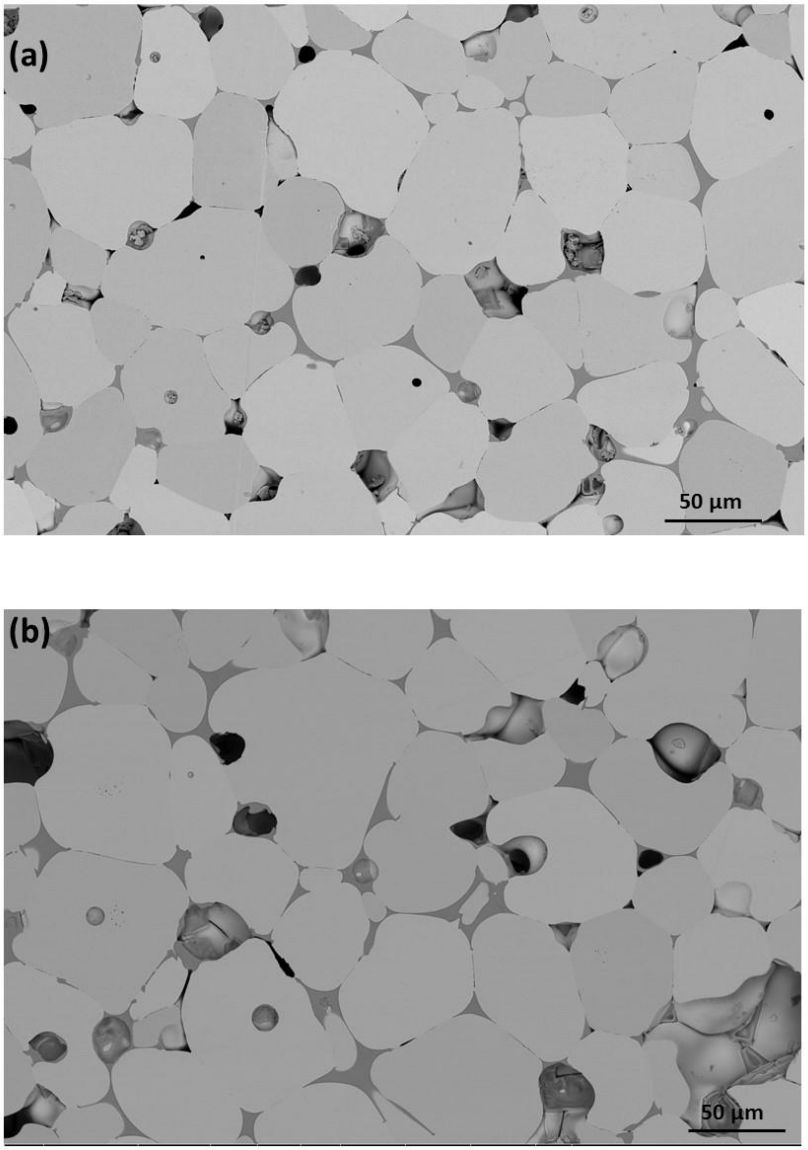


**Figure 7**: SEM images of (a) sample 3a ($UO_2$ pellet doped with **0.8 wt% $Nb_2O_5$/$NbO_2$**) and (b) sample 4a ($UO_2$ pellet doped with **1.6 wt% $Nb_2O_5$/$NbO_2$**), both sintered 3 h at 1670°C **in Ar**.

For these two samples, the composition of the Niobium precipitates was investigated using EDX. About 200 punctual analyses were performed in relatively large precipitates (to avoid any matrix contribution) randomly selected. **Fig. 8** represent an example of EDX line scans performed across Nb-rich precipitates. According to EDX punctual measurements in this sample, the precipitates consisted of a single Niobium oxide whose composition is U ~ 8 ± 1 at%, Nb ~ 22 ± 2 at% and O ~ 70 ± 1 at%, which is consistent with the $UNb_3O_{10}$ stoichiometry. This suggests that under Ar, both $NbO_2$ and $Nb_2O_5$ were converted into

$UNb_3O_{10}$ during sintering, according to the following reactions (assuming that the amount of Niobium dissolved into the $UO_2$ solid solution can be neglected):

$$NbO_2 + \frac{2-0.001}{3(x-0.001)} UO_{2+x} \rightarrow \frac{1}{3} UNb_3O_{10} + \frac{2-x}{3(x-0.001)} UO_{2.001} \quad (3)$$

$$Nb_2O_5 + \left(\frac{1}{3x} + \frac{0.002}{x}\right) UO_{2+x} \rightarrow \frac{2}{3} UNb_3O_{10} + \left(\frac{1}{3}\left(\frac{1}{x} - 2\right) + \frac{0.002}{x}\right) UO_{2.001} \quad (4)$$

with x~0.03 as the initial stoichiometry deviation of the uranium oxide before sintering. Equations (3) and (4) suggest that the precipitation of $UNb_3O_{10}$ has a reducing effect inside the pellets, as it implies conversion of some $UO_{2+x}$ into $UO_{2.001}$. This ($UNb_3O_{10}$) form has already been synthesized by mixing $U_3O_8$ and $Nb_2O_5/NbO_2$ in a sealed system heated at 1100°C during 40 hours [19]. This is consistent with our observations, which confirms that $UNb_3O_{10}$ is stabilized at high $pO_2$ compared to the $Nb_2O_5/NbO_2$ equilibrium at 1670°C.

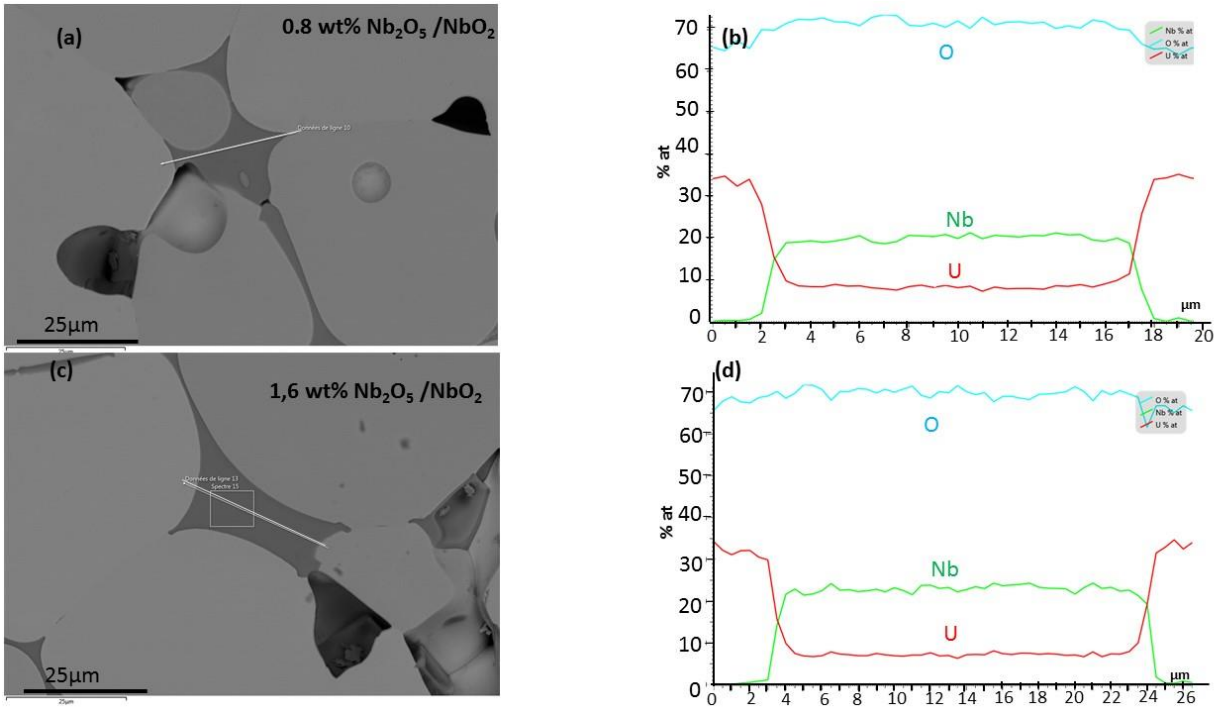


**Figure 8:** EDX line scan analysis of (a), (b) sample 3a ($UO_2$ pellets doped with **0.8 wt% $Nb_2O_5/NbO_2$**) and (c), (d) sample 4a ($UO_2$ pellets doped with **1.6 wt% $Nb_2O_5/NbO_2$**), both sintered 3 h at 1670°C **in Ar**.

### 3.2.2.2. Sintering under Ar/2% $H_2$ atmosphere

**Fig. 9** presents the X-ray diffraction patterns of Niobium powder loacted inside the crucible and in the furnace under Ar/2%$H_2$ atmosphere. Diffractogram (in black) shows the existence in the crucible of the $NbO_2$ and $Nb_2O_{5-x}$ ($Nb_{12}O_{29}$ and $NbO_{2.432}$) phases, which suggests that the $O_2$ partial pressure inside the crucible was stabilized in the vicinity of the ($NbO_{2.432}$/$NbO_2$) redox buffer. In contrast, as shown in **Fig. 9** (diffractogram in red), the $Nb_2O_5$ part of the buffer placed inside the furnace was completely reduced during sintering. It can be attributed to the reduction of $Nb_2O_5$ into $NbO_2$ by $H_2$ according to equilibrium (5):

$$Nb_2O_5 + H_2 \rightarrow 2NbO_2 + H_2O \qquad (5)$$

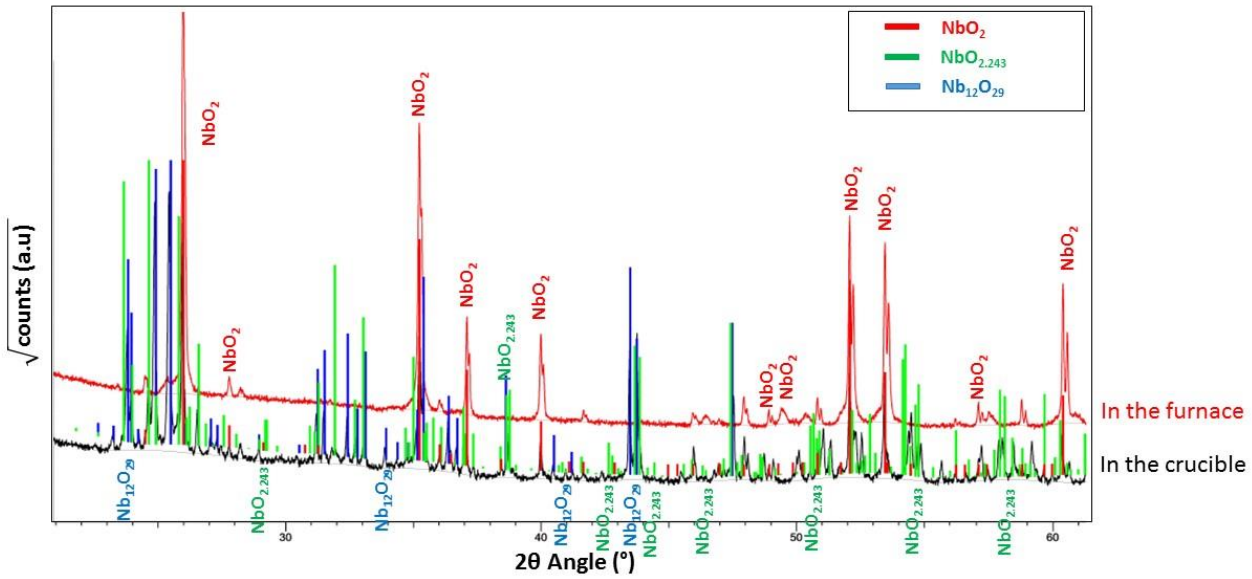


**Figure 9:** X-ray diffraction patterns of $Nb_2O_5$/$NbO_2$ powders sintered 3 h at 1670°C under Ar/2% $H_2$ in the furnace (red curve) and in the tungsten crucible (black curve). In the Y axes, the square root of the diffracted intensities is given.

The SEM images of samples 3b and 4b sintered at 1670°C in Ar/2%$H_2$ mixtures are shown in **Fig. 10 (a) & (b)** respectively. Conversely to what was observed for the sintering under Ar, the SEM micrographs clearly show three different shades of grey corresponding to three different phases. The light grey shade corresponds to $UO_2$ while the medium and dark grey shades refer to precipitates containing two different Niobium contents.

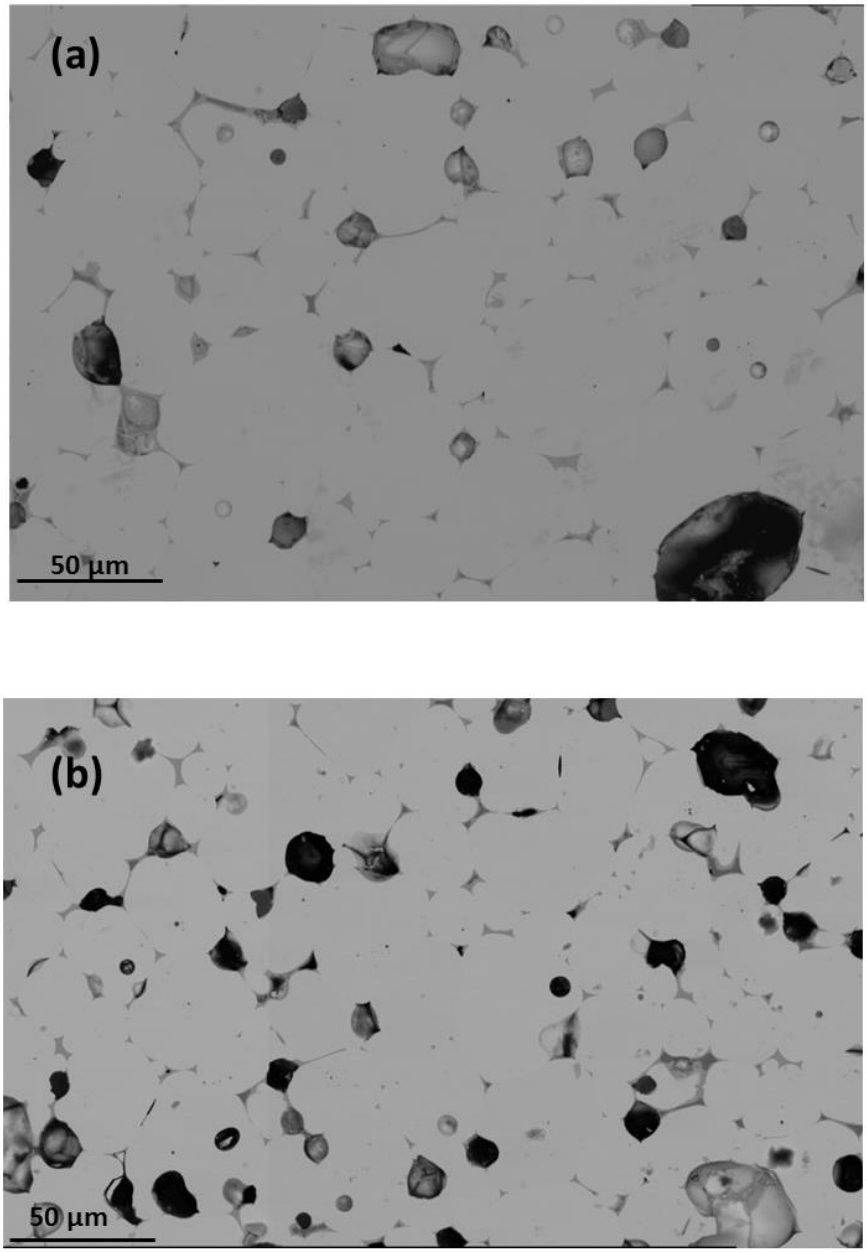


**Figure 10:** SEM images of (a) sample 3b ($UO_2$ pellet doped with **0.8 wt% $Nb_2O_5$/$NbO_2$**) and (b) sample 4b ($UO_2$ pellet doped with **1.6 wt% $Nb_2O_5$/$NbO_2$**), both sintered 3 h at 1670°C in **Ar/2% $H_2$**.

The EDX line scans (presented in **Fig. 11)** and 200 EDX punctual analyses (see **Table 3**) reveal that the dark grey shade corresponds to $NbO_2$ precipitates (in agreement with the Nb ~ 35 ± 1 at% and O ~ 64 ± 1 at% composition), in both samples (0.8 and 1.6 wt% Nb). The medium grey phase present in both pellets corresponds to the following composition as provided by the EDX analysis: U ~11 ± 1 at%, Nb ~22 ± 1 at% and O ~67 ± 1 at%). Therefore, it can be attributed to $UNb_2O_6$ or $UNb_2O_7$. Identifying the real composition is tricky especially knowing that the accuracy of the EDX analysis is 1 to 2 at%. However,

since $UNb_2O_7$ is a known stable phase in the U-Nb-O system [18], [19] we assume that this composition corresponds to the $UNb_2O_7$ phase.

At this stage, the buffer ($NbO_2/UNb_2O_7$) is likely to control the $O_2$ partial pressure inside the pellets according to the following equilibrium (neglecting Nb solubility into $UO_2$):

$$UNb_2O_7 \rightarrow 2NbO_2 + UO_{2+\varepsilon} + \frac{1}{2}(1-\varepsilon)O_2 \quad (6)$$

The buffering capacity of this system is of about ¼ mol $O_2$/mol Nb. However, the difference between the quantities of both precipitates could indicate that the equilibrium state is not yet reached for those samples.

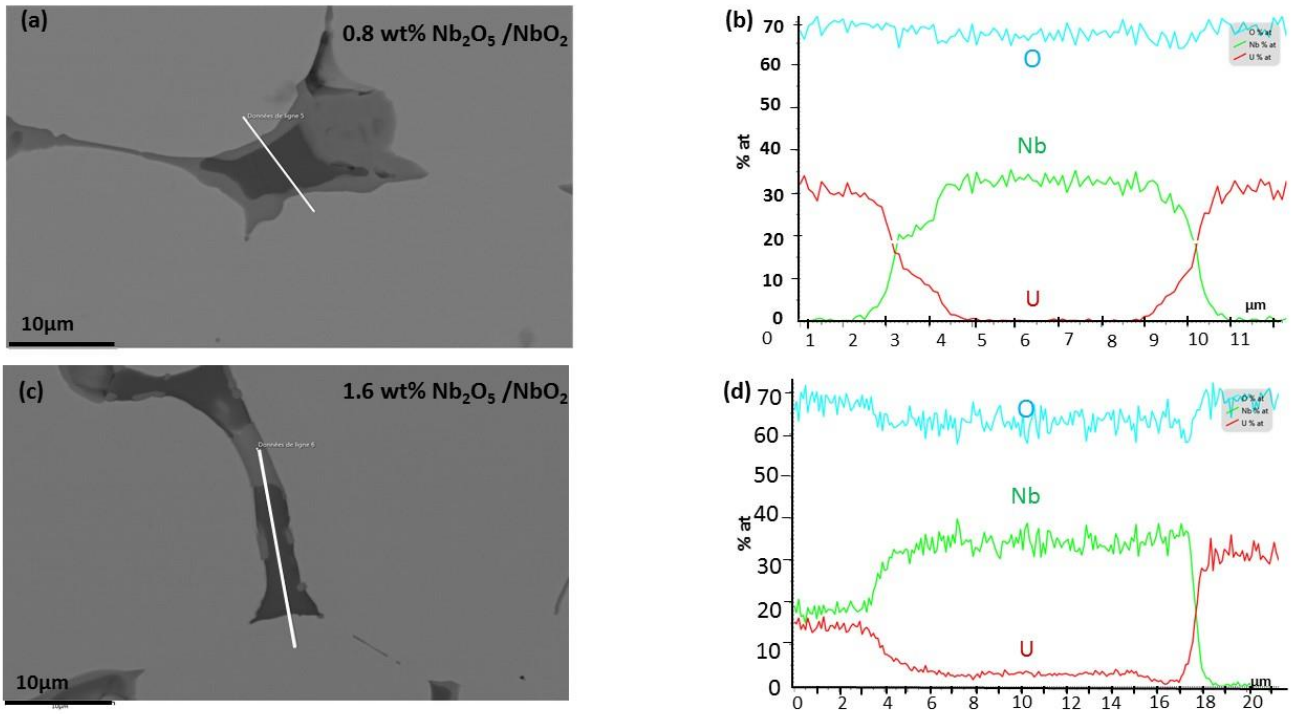


**Figure 11:** EDX line analysis of (a), (b) sample 3b ($UO_2$ pellets doped with **0.8 wt% $Nb_2O_5/NbO_2$**) and (c), (d) sample 4b ($UO_2$ pellets doped with **1.6 wt% $Nb_2O_5/NbO_2$**), both sintered 3 h at 1670°C in **Ar/2% $H_2$**.

### 3.2.2.3. Sintering under Ar/5% $H_2$ atmosphere

For the buffer placed inside the crucible, XRD analysis **(Fig.12 (diffractogram in red),** performed after sintering under the most reducing conditions, showed the presence of the same crystallographic phases, $NbO_2$ and $Nb_2O_{5-x}$ ($Nb_{12}O_{29}$ and $NbO_{2.432}$) as those found previously when the sintering was performed

under Ar and Ar 2%$H_2$. In addition, as shown in **Fig. 12 (diffractogram in black)**, the $Nb_2O_5$ part of the buffer placed inside the furnace completely disappeared, being reduced during sintering, according to the following reactions:

$$Nb_2O_5 + H_2 \rightarrow 2NbO_2 + H_2O \quad (7)$$

$$2NbO_2 + H_2 \rightarrow Nb_2O_3 + H_2O \quad (8)$$

$$Nb_2O_3 + H_2 \rightarrow 2NbO + H_2O \quad (9)$$

As expected, the (Ar/5 % $H_2$) gas flow being more reducing than the (Ar/2% $H_2$) one, more reduced phases of Niobium ($NbO_2$ + $Nb_2O_3$ + NbO) were formed in the buffer in the furnace as compared to the test performed under (Ar/2% $H_2$) gas flow (only $NbO_2$). Nevertheless, the $O_2$ partial pressure was kept stable inside the crucible, as it is still controlled by the ($NbO_{2.432}$/$NbO_2$) redox buffer whatever the initial atmosphere composition. The system is obviously not at equilibrium at the end of the 3-hours sintering step. However, the results indicate that $H_2$ helped reducing the initial hyperstoichiometric uranium oxide powder so as to obtain in the end a sintered pellet containing two oxido-reducing forms of Nb ($NbO_2$ and $UNb_2O_7$), which are thus likely to control *in situ* the oxygen potential of the pellet.

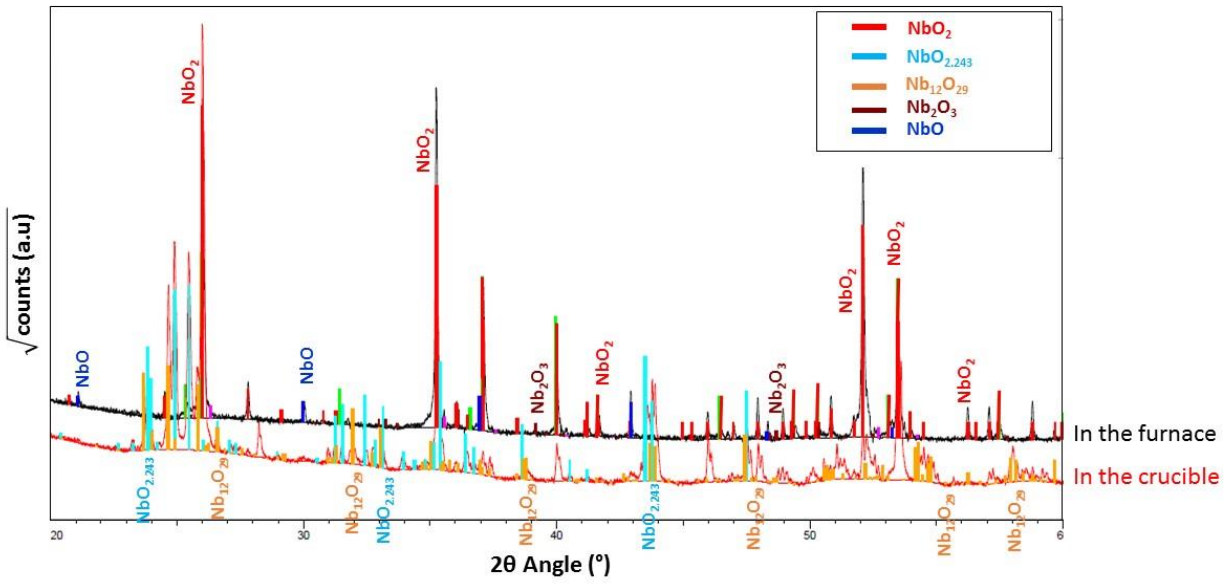


**Figure 12:** X-ray diffraction patterns of $Nb_2O_5$/$NbO_2$ powders sintered 3 h at 1670°C under Ar/5% $H_2$ in the furnace (black curve) and in the tungsten crucible (red curve). In the Y axes, the square root of the diffracted intensities is given.

The SEM images of samples 3c and 4c ($UO_2$ pellets doped with 0.8 and 1.6 wt% Nb) annealed at 1670°C in Ar/5% $H_2$ (**Fig. 13**) show that the pellets are closer to equilibrium, which was also verified by the homogeneity of the precipitates. The associated EDX line scans (presented in **Fig. 14)** and 200 EDX punctual analyses (see **Table 3**) are consistent with the co-existence of two Niobium oxide precipitates of stoichiometry $NbO_2$ (in consistency with the composition Nb ~ 35 ± 1 at% and O ~ 64 ± 1 at%), and $UNb_2O_7$ (in consistency with the composition U ~11 ± 1 at%, Nb ~22 ± 1 at% and O ~68 ± 1 at%). At this stage, the ($UNb_2O_7$/$NbO_2$) buffer is likely to control the $O_2$ partial pressure inside the pellets according to the equilibrium (5) with the same buffering capacity of 1/4 mol $O_2$/mol Nb.

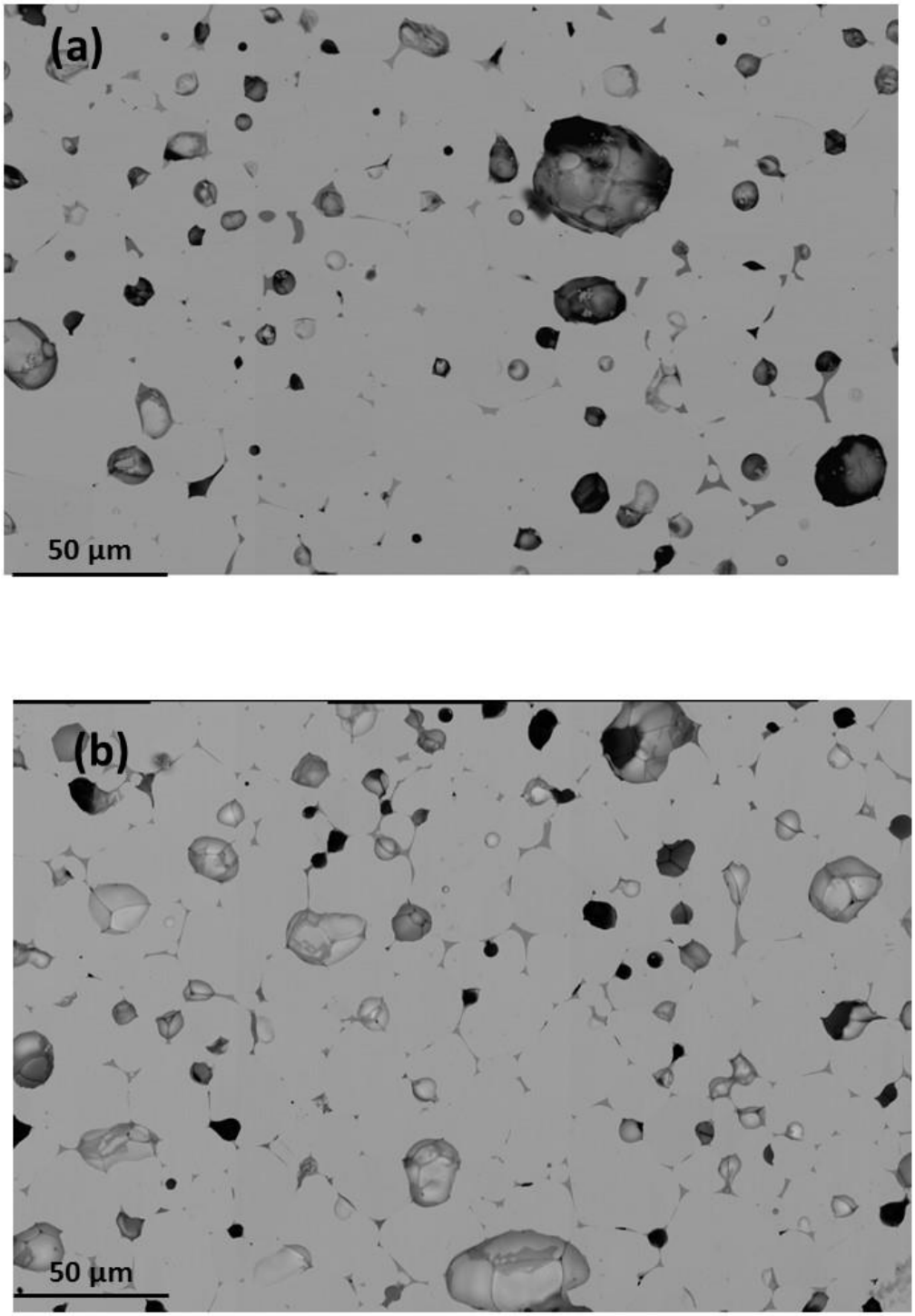


**Figure 13:** SEM images of (a) sample 3c ($UO_2$ pellet doped with **0.8 wt% $Nb_2O_5$/$NbO_2$**) and (b) sample 4c ($UO_2$ pellet doped with **1.6 wt% $Nb_2O_5$/$NbO_2$**), both sintered 3 h at 1670°C in **Ar/5% $H_2$**.

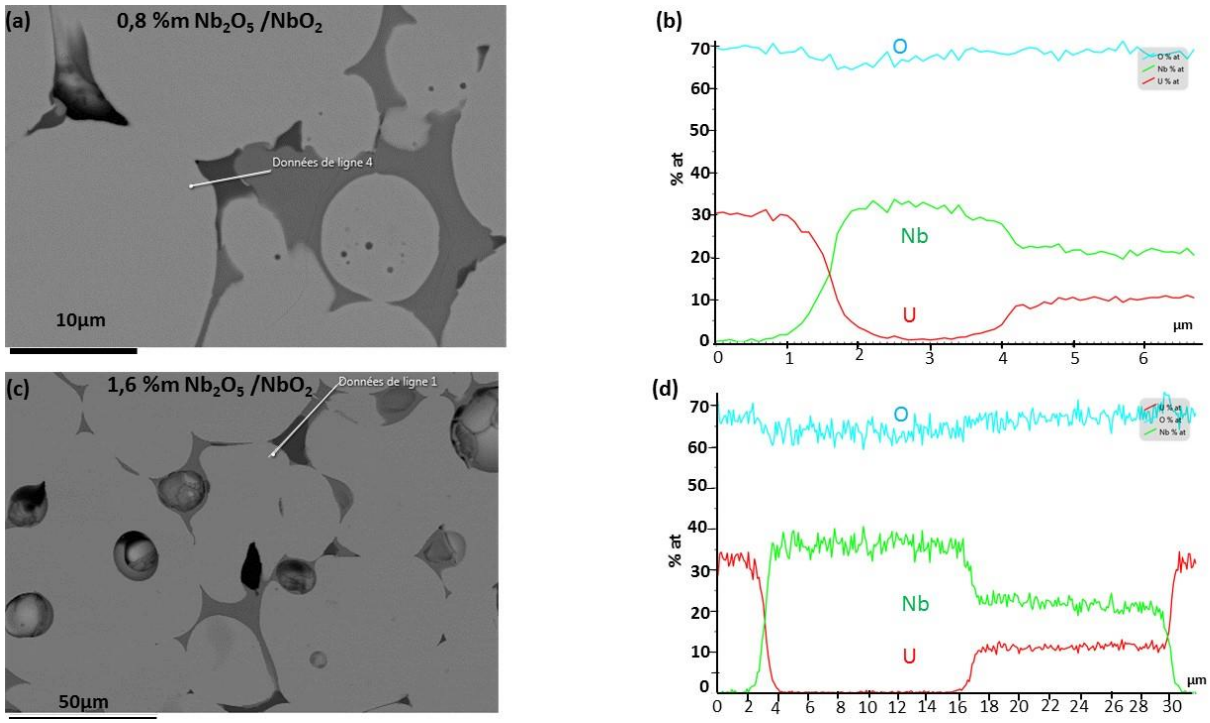


**Figure 14:** EDX line analysis of (a), (b) sample 3c ($UO_2$ pellets doped with **0.8 wt% $Nb_2O_5$/$NbO_2$**) and (c), (d) sample 4c ($UO_2$ pellets doped with **1.6 wt% $Nb_2O_5$/$NbO_2$**), both sintered 3 h at 1670°C in **Ar/5% $H_2$**.

Also, for these pellets, it was interesting to see the effect of the $UNb_2O_7/NbO_2$ couple on $UO_2$ grain growth. EBSD maps were taken across the cross-section of the pellet as indicated in **Fig. 15**. The different colors reveal different crystal orientations, while the black spots represent pores (positions for which crystallographic orientations failed to be indexed). The EBSD data were analyzed assuming that the minimal grain size is 5 µm. Thus, the average grain size was determined as 38 µm, higher than the conventional grain size of $UO_2$ sintered in the same conditions (~ 10 µm). Furthermore, we can clearly see in the figure the homogeneity of grain size between the center and the edge of the pellet.

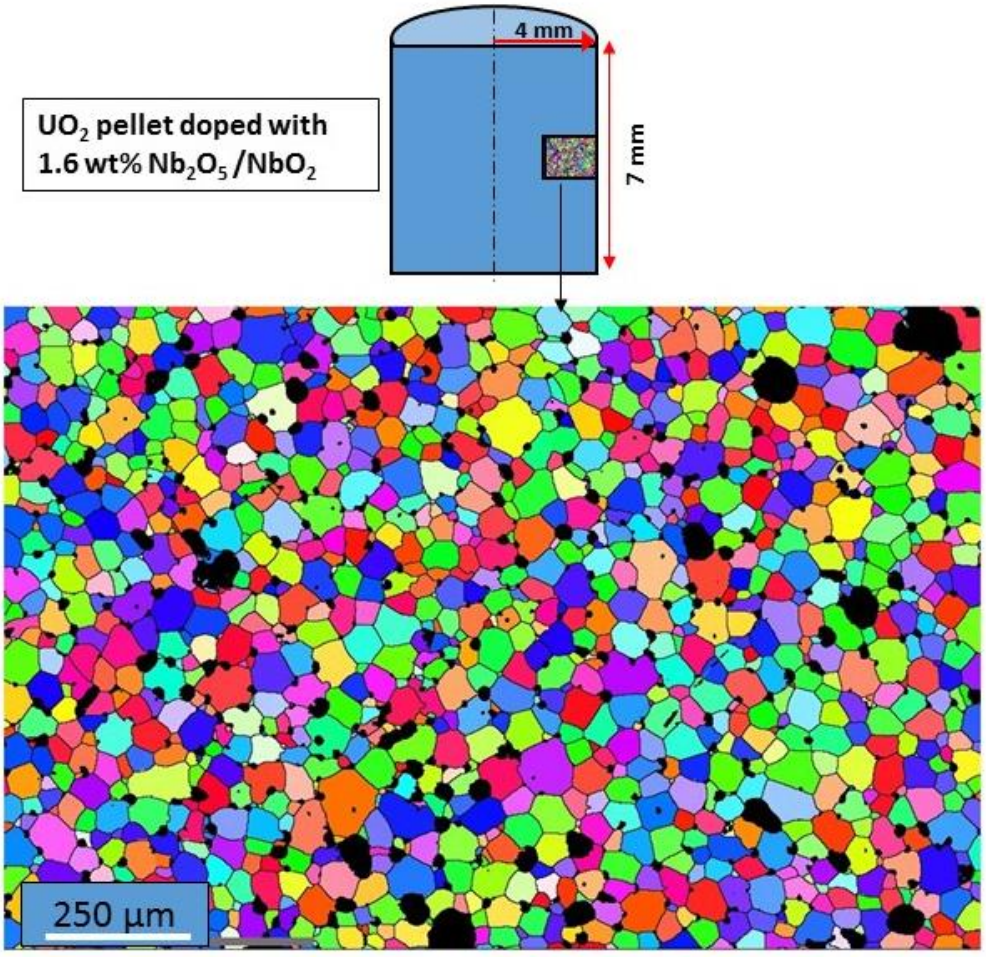


**Figure 15:** SEM picture of grains of sample 4c ($UO_2$ doped with 1.6 wt% $Nb_2O_5/NbO_2$) sintered 3 h at 1670°C in **Ar/5% $H_2$**.

# 4. Discussion

In order to understand the chemical evolution of the different ($MoO_2$/Mo, $Nb_2O_5/NbO_2$) couples introduced as solid buffers in $UO_2$ to control *in situ* the $pO_2$, the EDX and XRD analysis results are summarized in Tables 4 and 5. The elemental compositions of each sample of $UO_2$ doped Niobium (sample 4) are given in **Table 4**. Although TEM (Transmission Electron Microscopy) or EPMA (Electron probe micro-analyzer) were not used, the proposed stoichiometries of the obtained U-Nb oxides could be considered as robust due to the high number of measurements performed. In addition, **Table 5** summarizes the phase compositions of all buffer-doped $UO_2$.

As a matter of fact, it shows that the external buffers play a major role in controlling the redox conditions during sintering.

| Gas in the furnace | Precipitates Grey level | Number of spot analysis | Concentration (at%) & *standard deviation* | | | Final composition |
|---|---|---|---|---|---|---|
| | | | **U** | **Nb** | O | |
| Ar | Medium | 186 | **8** ± *1* | **22** ± *1* | **70** ± *1* | $UNb_3O_{10}$ |
| Ar 2% $H_2$ | Medium | 253 | **11** ± *1* | **22** ± *1* | **67** ± *1* | $UNb_2O_7$ |
| | Dark | 110 | **0** | **35** ± *1* | **64** ± *1* | $NbO_2$ |
| Ar 5% $H_2$ | Medium | 200 | **11**± *1* | **21** ± *1* | **68** ± *1* | $UNb_2O_7$ |
| | Dark | 113 | **0** | **35** ± *1* | **64** ± *1* | $NbO_2$ |

| Buffer | Atmosphere | Buffer powder in the furnace (XRD) | Buffer powder in the crucible (XRD) | Precipitates (EDX) |
|---|---|---|---|---|
| **Molybdenum** | **Ar** | $MoO_2$/Mo | $MoO_2$/Mo | $MoO_2$/Mo |
| **Niobium** | **Ar** | $Nb_2O_{5-x}/NbO_2$ | $Nb_2O_{5-x}/NbO_2$ | $UNb_3O_{10}$ |
| | **Ar/2 %$H_2$** | $NbO_2$ | $Nb_2O_{5-x}/NbO_2$ | $NbO_2/UNb_2O_7$ |
| | **Ar/5 %$H_2$** | $NbO_2/Nb_2O_3$/NbO | $Nb_2O_{5-x}/NbO_2$ | $NbO_2$ /$UNb_2O_7$ |

Concerning Mo based buffers, a mixture of $MoO_2$ and Mo precipitates was observed in all pellets when using external $MoO_2$/Mo buffer in Ar atmosphere regardless of the concentration of the internal buffer. This indicates that the $pO_2$ inside the system was well controlled.

Concerning Nb based buffers, the chemical response is more complex. In that case, the amount of buffer is not sufficient to ensure the pre-reduction of the $UO_{2.03}$, before sintering. As stated in **Section 2.1**, 2.7 wt% should be necessary and only 1.6 wt% at maximum was added. Therefore, in a non-reducing atmosphere such as Ar, $NbO_2$ initially present into the pellets, was totally oxidized into $UNb_3O_{10}$ in order to reduce the initial $UO_{2.03}$. Indeed, only $UNb_3O_{10}$ precipitates were observed. In order to preserve both oxido-reducing forms of Nb inside the pellets, it is therefore necessary to use either $H_2$ in the sintering atmosphere or a pre-reduced $UO_{2.00}$ powder instead of $UO_{2.03}$. Actually, when the sintering atmosphere was Ar 2%$H_2$ or Ar 5%$H_2$, a mixture of $UNb_2O_7$ and $NbO_2$ precipitates was observed, regardless of the concentration of the internal buffer. Under these conditions, the internal buffer allowed controlling $pO_2$ within the pellets. However, it should be noted that the observed precipitates were different from those

(NbO and $NbO_2$) obtained in [5] in similar experimental conditions but without any external buffer. This confirms the importance of the external buffer in controlling the $pO_2$ during sintering. Finally, although changes in the precipitate composition were observed as a function of the sintering atmosphere, the initial composition inside the crucible remained the same ($Nb_2O_{5-x}/NbO_2$) after sintering, while the buffer in the furnace changed with the atmosphere. This confirms that our system was semi-isolated. Using a sealed system can be a good replacement of the semi-closed one but would prevent using hyperstoichiometric $UO_2$ ($UO_{2.03}$). One should add that the presence of both forms of Niobium oxides ($Nb_2O_{5-x}/NbO_2$) in the crucible after sintering shows that there were sufficient amounts of buffer components to control this $pO_2$.

**Fig. 16** summarizes the equilibrium redox conditions achieved by the Molybdenum and Niobium samples during sintering. In fact, the figure shows the stability areas of the various compounds of the Mo-Nb-U-O system in "a RTLn ($pO_2$) versus T" diagram, based on the TAFID thermodynamic database [20]. The Mo specimens sintered under Ar flow as well as the Nb specimens sintered under (Ar / 2% $H_2$) or (Ar / 5% $H_2$) incorporate two oxido-reducing forms of the dopant after sintering, which implies the $O_2$ partial pressure is *in situ* controlled by the corresponding redox buffers, ($MoO_2$/Mo) and ($UNb^{V}_2O_7/Nb^{IV}O_2$) respectively. Above 1500°C, the Nb redox system incorporated in $UO_2$ is in liquid phase, with a ratio $Nb^{5+}/Nb^{4+}$ between the two major redox species varying between 0.9 and 0.95, as estimated using the TAFID database.

The figure gives evidence of the interest of using selected solid redox buffers to produce $UO_2$ specimens evolving under strictly controlled redox potentials, representative of irradiated nuclear fuels (approximately between the ($MoO_2$/Mo) couple and $UO_{2.000}$).

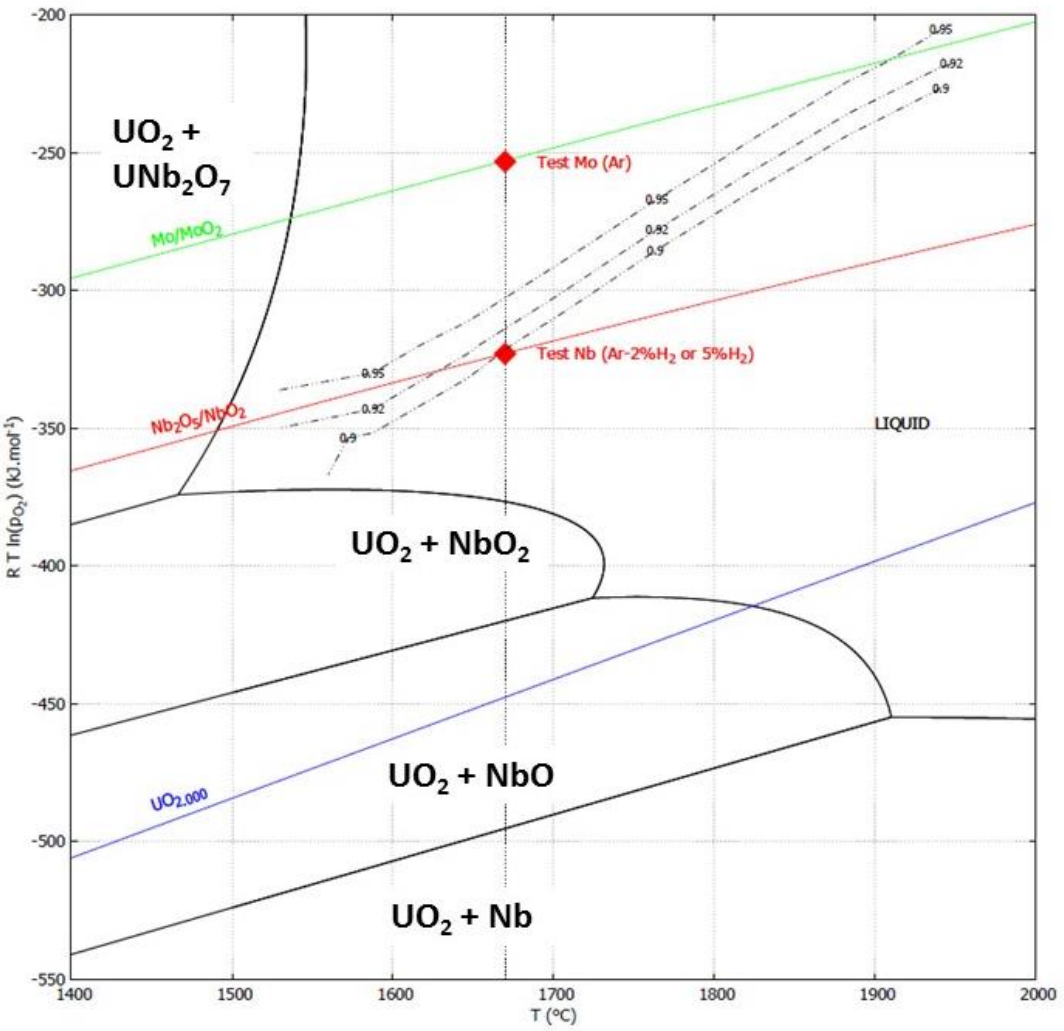


**Figure 16:** Stability diagram of the Nb-U-O system, calculated with Thermocalc using the TAFID thermodynamic database [20].

The dashed lines in the Liquid area show curves with constant ($Nb^{5+}/Nb^{4+}$) ratio, as indicated on labels. The red squares show the equilibrium conditions achieved by the samples during sintering (cf. Table 4).

Finally, it is worth mentioning the impact of the Niobium buffer on the microstructure, which caused a significant increase in the grain size (from 10 to ~40 µm). This is due to the presence from about 1500°C of a liquid phase for $UNb_2O_7$ which is able to activate the $UO_2$ grain growth via liquid phase transport. On the contrary, the sintering temperature does not authorize a liquid phase for $Mo/MoO_2$. In addition, according to [21], the very low solubility of Mo in $UO_2$ (0.002 at% [6]) implies a very low presence of Mo in $UO_2$ interstitial sites. Thus, it should not impact largely the diffusivity of Uranium during sintering

nor grain growth. This is consistent with the very low grain growth observed in the sample buffered with the $MoO_2$/Mo couple.

# 5. Conclusion

$UO_2$-doped pellets were successfully manufactured with an innovative route making use of the specific properties of solid redox buffers. The method simply consists in mixing the $UO_2$ powder with the selected redox buffer and then sintering the pellets in a quasi-closed vessel with a controlled $O_2$ partial pressure. The strict control of sintering atmosphere was achieved by pre-equilibrating the flowing gas with solid redox buffers of same composition as that incorporated in the pellets. In the case of Nb based buffer, the initial overstoichiometry of $UO_2$ should be taken into account to avoid the oxidation of the reducing element of the buffer inside the pellet. The use of a more reducing atmophere than Ar, such as an Ar/$H_2$ gas mixture, allows then the preservation of both forms of Nb inside the pellets. Using a sealed system can be also a good replacement of the semi-closed one. Some improvements are still needed however such as the densification procedure (sintering temperature and duration [5], [22], [23]) in order to obtain high density pellets.

Oxido-reduction playing a central role on the behavior of irradiated nuclear fuels, this achievement is an important step opening the path to laboratory in-depth studies on the impact of oxido-reduction on the key properties of irradiated fuels, especially the speciation of minor fission products such as I, Te and Cs responsible for some cladding corrosion phenomena.

**Acknowledgments**

The authors would like to thank Framatome and EDF for their financial and technical support in this study. Technical support by F. GAREL is also gratefully acknowledged.

**References:**


[1] Ch. Riglet-Martial *et al.*, « Experimental evidence of oxygen thermo-migration in PWR $UO_2$ fuels during power ramps using in-situ oxido-reduction indicators », *J. Nucl. Mater.*, vol. 480, p. 32-39, Nov. 2016.

[2] B. Baurens, « Couplages thermo-chimie mécaniques dans le dioxyde d'uranium : application à l' intéraction pastille-gaine », PHD, Aix-Marseille, 2014.

[3] B.Baurens et al., « 3D thermo-chemical–mechanical simulation of power ramps with ALCYONE fuel code », *J. Nucl. Mater*, vol. 452, nº 1-3, p. 578-594, sept. 2014.

[4] T. Muromura *et al.*, « Oxygen potential self-control type nuclear fuel compound », JPH06258477A, 16-Sept-1994.

[5] V. Pennisi, « Contribution à l'identification et à l'évaluation d'un combustible $UO_2$ dopé à potentiel oxygène maîtrisé », PHD, Université de Bordeaux, 2015.

[6] H. Kleykamp, « The chemical state of the fission products in oxide fuels », *J. Nucl. Mater.*, vol. 131, nº 2, p. 221-246, April 1985.

[7] C. Riglet-Martial, M. Brothier, P. Matheron, V. Pennisi, et V. Basini, « Oxide nuclear fuel which is a regulator of corrosive fission products, additivated with at least one oxidation-reduction system », Patent WO2014072463A1, 15-May2014.

[8] H. Khedim, « Etude de la limite de solubilite de la chromine « $Cr_2O_3$ » dans les liquides silicates – determination de grandeurs thermodynamique et physico-chimique », University of Lorraine, 2008.

[9] T. Arima, T. Masuzumi, H. Furuya, K. Idemitsu, et Y. Inagaki, « Reaction of Zircaloy-4 with tellurium under different oxygen potentials », *J. Nucl. Mater*, vol. 301, nº 2, p. 90-97, March 2002.

[10] M. Körner, M. Schulz, H. Fritze, et Ch. Stenzel, « Control of partial pressure of oxygen in the ppm range based on a two metal–oxide buffer system », *Sens. Actuators B Chem.*, vol. 190, p. 702-706, Jan. 2014.

[11] Y. Harada, « Sintering behaviour of niobia-doped large grain $UO_2$ pellet», *J. Nucl. Mater.*, vol. 238, nº 2, p. 237-243, Nov. 1996.

[12] J.e. Killeen, « The densification and grain growth of $UO_2$ doped with $Nb_2O_5$ », *CEGB Rep. No. RD/B/N3374, 1976*, 1976.

[13] K. Yanagisawa, « Behavior of $Nb_2O_5$ Doped $UO_2$ Fuel in Reactivity Initiated Accident Conditions », *J. Nucl. Sci. Technol.*, vol. 28, nº 5, p. 459-471, May 1991.

[14] K.-W. Song, K.-S. Kim, K.-W. Kang, et Y.-H. Jung, « Effects of $Nb_2O_5$ , and Oxygen Potential on Sintering Behavior of $UO_2$ Fuel Pellets », *Nucl. Eng. Technol.*, vol. 31, nº 3, p. 335-343, 1999.

[15] J. F. Marucco, « Thermodynamic study of the system $NbO_2$-$Nb_2O_5$ at high temperature », *J. Solid State Chem.*, vol. 10, nº 3, p. 211-218, july1974.

[16] H. Schäfer, D. Bergner, et R. Gruehn, « Beiträge zur Chemie der Elemente Niob und Tantal. LXXI. Die thermodynamische Stabilität der sieben zwischen 2,00 und 2,50 O/Nb existierenden Phasen », *Z. Für Anorg. Allg. Chem.*, vol. 365, nº 1-2, p. 31-50, 1969.

[17] C. Nico, T. Monteiro, et M. P. F. Graça, « Niobium oxides and niobates physical properties: Review and prospects », *Prog. Mater. Sci.*, vol. 80, p. 1-37, July. 2016.

[18] C. Miyake, S. Ohana, S. Imoto, et K. Taniguchi, « Oxidation states of U and Nb in U-Nb-O ternary oxides by means of magnetic susceptibility, XPS and ESR », *Inorganica Chim. Acta*, vol. 140, p. 133-135, Dec. 1987.

[19] C. Keller, « Die reaktion der dioxide der elemente thorium bis americium mit niob- und tantalpentoxid », *J. Inorg. Nucl. Chem.*, vol. 27, nº 6, p. 1233-1246, June 1965.

[20] C. Guéneau *et al.*, « A thermodynamic approach for advanced fuels of gas-cooled reactors », *J. Nucl. Mater*, vol. 344, nº 1, p. 191-197, Sept. 2005.

[21] M. W. D. Cooper, C. R. Stanek, et D. A. Andersson, « The role of dopant charge state on defect chemistry and grain growth of doped $UO_2$ », *Acta Mater.*, vol. 150, p. 403-413, May 2018.

[22] D. Bernache-Assollant et J.-P. Bonnet, « Frittage : aspects physico-chimiques - Partie 1 : frittage en phase solide », p. 25, 2005.
[23] P. Balakrishna, B. Narasimha Murty, K. P. Chakraborthy, R. N. Jayaraj, et C. Ganguly, « Coarsening-densification transition temperature in sintering of uranium dioxide », *J. Nucl. Mater.*, vol. 297, n° 1, p. 35-42, July 2001.